Theoretical studies of enhanced anomalous Nernst effect in Fe_3Ga

Ondřej Stejskal *
Faculty of Mathematics and Physics, Charles University, Ke Karlovu 5, Prague, Czech Republic and Institute of Physics, The Czech Academy of Sciences, Na Slovance 2, Prague, Czech Republic

Martin Veis and Jaroslav Hamrle
Faculty of Mathematics and Physics, Charles University, Ke Karlovu 5, Prague, Czech Republic

(Received 19 January 2023; accepted 7 July 2023; published 8 August 2023)

The anomalous Nernst effect (ANE) is a member of the extensive family of topological effects in solid state physics. It converts a heat current into electric voltage and originates from the Berry curvature of electronic bands near the Fermi level. Recent results established the Fe_3Ga alloy as one of the most promising candidates for applications, due to its flat band structure consisting of a rich web of nodal lines. In this theoretical work, we study the effect of deformation of Fe_3Ga on the anomalous Nernst effect, which naturally occurs in thin films. Furthermore, we demonstrate that doping, which effectively shifts the position of the Fermi level, can also significantly modify the strength of the effect. Lastly, we provide detailed analysis of the origin of ANE in the electronic structure of Fe_3Ga which yields a deeper insight into the generating mechanisms, the understanding of which can lead to substantial enhancement of the effect in the future.

DOI: 10.1103/PhysRevMaterials.7.084403

I. INTRODUCTION

In recent years, topological effects have attracted a lot of attention in solid state research, due to their unique and interesting manifestations with an enormous potential in applications. In magnetic materials, broken time-reversal symmetry induces anomalous linear response effects such as the anomalous Hall effect [1–5], anomalous Nernst effect (ANE) [6,7], and magneto-optic Kerr effect [8,9], all being governed by the presence of the Berry curvature of the electronic states.

ANE manifests itself as thermoelectricity, i.e., lossless conversion of heat flow into electricity, which plays a key role in developing novel energy-harvesting technologies. The transverse geometry of the effect in ferromagnets offers many advantages to the conventional longitudinal Seebeck effect [10,11], but is significantly smaller in magnitude. Currently, huge effort is devoted to searching and identifying materials providing large ANE at zero field.

It has been discovered that ANE originates from the Berry curvature of the conduction electrons at the Fermi level [2] and is strongly enhanced with the presence of nodal lines and planes for bands at the Fermi level which are then split by the spin-orbit interaction (SOI) to provide large Berry curvatures [12–20]. Therefore, an extensive amount of high-throughput first-principle calculations were performed in order to find materials with large nodal structures and high density of states at the Fermi energy.

The research has shifted toward ferromagnetic Heuslers [17,21], Fe_3X alloys [18,19,22] lately, with Fe_3Ga coming out on top [18,23] due to its rich flat band structure at Fermi energy in the vicinity of point L. This material has been calculated before [18,24] but limited only to stoichiometric undeformed cubic structure.

In this work, we investigate how modifications of the crystal structure of Fe_3Ga by both deformation and doping affect the value of ANE. We show that compressive strain is to be sought for in thin film applications.

Furthermore, the electronic structure of DO_3-ordered Fe_3Ga is thoroughly studied in order to identify the underlying origin of its large ANE. Two distinct sources of the effect are identified in the Brillouin zone (BZ) and analyzed separately.

II. ELECTRONIC STRUCTURE OF Fe_3Ga

The electronic structure of DO_3-ordered Fe_3Ga bulk crystal [Fig. 1(a)] was calculated by the WIEN2k code [25,26] with 27 000 k points in the full Brillouin zone and the generalized gradient approximation [27] as the exchange-correlation potential. The lattice constant was set to 5.80 Å [28]. The calculation was performed with the spin-orbit interaction and with magnetization in the z direction. The product of the smallest atomic sphere and the largest reciprocal space vector was set to $R_{\mathrm{MT}}K_{\max} = 7$ with the maximum value of the partial waves inside the spheres $l_{\max} = 10$. States up to $3s$ are treated as core states. Bands in Fig. 1(a) are labeled by an increasing energy eigenvalue starting with $3d$ Fe states. The closest Ga states are located approximately 7 eV below the Fermi level (see Fig. S5 in the Supplemental Material [29]).

The Berry curvature is calculated directly from the WIEN2k output by the Kubo-like formula:

$$\Omega^n_{\mu\nu}(\mathbf{k}) = -\frac{\hbar^2}{m^2}\sum_{n'\neq n}\frac{2\mathrm{Im}\,\langle\psi_{n\mathbf{k}}|\,p_\mu\,|\psi_{n'\mathbf{k}}\rangle\,\langle\psi_{n'\mathbf{k}}|\,p_\nu\,|\psi_{n\mathbf{k}}\rangle}{(E_n - E_{n'})^2}, \quad (1)$$

*stejskal@karlov.mff.cuni.cz

 ©2023 American Physical Society

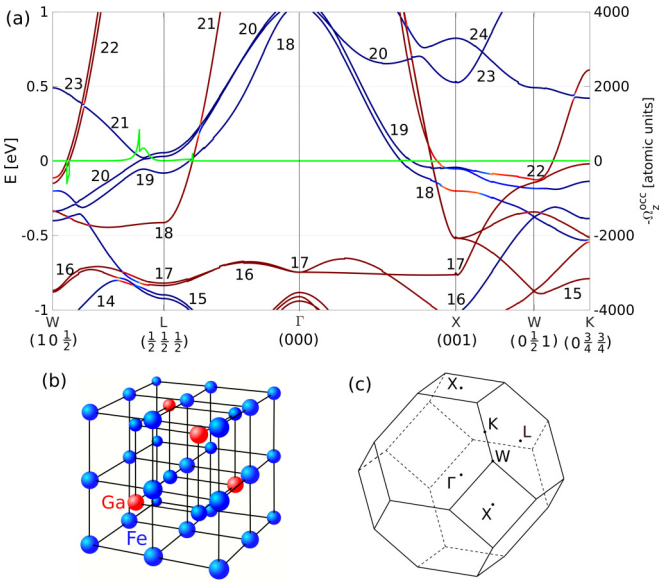

FIG. 1. (a) Band structure of DO_3-ordered Fe_3Ga crystal. Red (blue) color corresponds to spin down (up). Bands are indexed by their increasing energy eigenvalue starting with $3d$ Fe bands. SOI is included. The green curve corresponds to the z component of the Berry curvature over occupied states $\Omega_z^{occ} = \Sigma_n f_n \Omega_z^n$. (b) Crystal structure of Fe_3Ga. (c) Brillouin zone of fcc crystal.

where E_n is the band energy, $\psi_{n\mathbf{k}}$ are Bloch wave functions, and p_μ are momentum operators. The Berry curvature $\Omega_{\mu\nu}$ is an antisymmetric tensor that in three dimensions can be expressed in a pseudovector form via $\Omega_{\mu\nu} = \epsilon_{\mu\nu\xi}\Omega_\xi$. The calculation of the anomalous Hall conductivity (AHC) is carried out by integration of the Berry curvature over the Brillouin zone:

$$\sigma_{xy}^{\mathrm{AHE}} = -\frac{e^2}{\hbar}\frac{1}{(2\pi)^3}\sum_n \int_{\mathrm{BZ}} f_n(\mathbf{k})\Omega_z^n(\mathbf{k})\, d\mathbf{k}, \qquad (2)$$

where f is the Fermi-Dirac distribution function. This is nowadays a well-established procedure for evaluating the intrinsic part of the anomalous Hall conductivity [1–5].

The strength of the ANE is evaluated by the temperature-dependent anomalous transverse thermoelectric coefficient:

$$\alpha_{xy}(T) = -\frac{1}{e}\int dE\left(-\frac{\partial f}{\partial E}\right)\sigma_{xy}^{\mathrm{AHE}}(E)\frac{E}{T}. \qquad (3)$$

The anomalous Hall conductivity $\sigma_{xy}^{\mathrm{AHE}}(E)$ becomes a function of energy E that represents the threshold for which the electron states are treated as occupied. AHC is required to be calculated in a narrow energy interval in the vicinity of the Fermi level; therefore even minor changes in the form of doping and deformation can modify the value of ANE significantly.

A. Doping

The electronic structure of doped Fe_3Ga was modeled by the virtual crystal approximation. It is implemented by replacing Ga with a virtual element having a noninteger atomic number, which simulates an effective increase or decrease of electron density. Six alloys were considered substituting 5%, 10%, and 20% of Ga elements by either Ge or Zn.

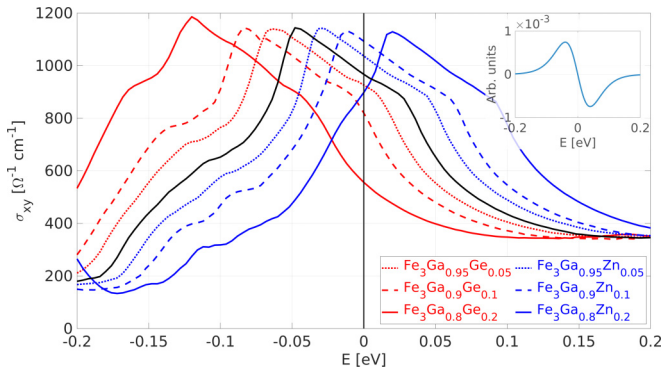

FIG. 2. AHC spectrum for doped Fe_3Ga crystal structure. In the inset, the weighting function for evaluation of α is shown.

From Fig. 2, it is apparent that doping effectively moves the position of the Fermi energy as the Ga states are buried deeply below the Fermi level. Substituting Ga with a heavier element (Ge) leads to a significant increase of the effect (see Table I) while a lighter element (Zn) kills the effect and with a higher concentration even changes its sign.

In the inset of Fig. 2 the evaluation at 300 K of the function entering the convolution [Eq. (3)] is depicted. This function weights the value of the anomalous Hall conductivity $\sigma_{xy}^{\mathrm{AHE}}(E)$ in the vicinity of the Fermi level to obtain the value of α. For correct numerical evaluation $\sigma_{xy}^{\mathrm{AHE}}(E)$ needs to be calculated in the energy interval from -0.2 eV to 0.2 eV.

The temperature dependence of the anomalous transverse thermoelectric coefficient α [Eq. (3)] for extreme cases is shown in Fig. 3. The values of $\alpha_{\max}$ [defined as the maximal value of $\alpha_{xy}(T)$] and $\alpha(300\ \mathrm{K})$ are presented in Table I. Generally, the value of α turns out to be very sensitive on the exact position of the Fermi level. Different *ab initio* codes and applied potentials result in different values of the Fermi energy, making it a very difficult parameter to obtain from first principles alone. Sakai *et al.* [18] reported $\alpha_{\max} = 3.0\ \mathrm{A\,K^{-1}\,m^{-1}}$ for Fe_3Ga. We arrive at the same value if we adjust the Fermi level to match theirs.

TABLE I. Thermoelectric coefficients $\alpha_{\max}$ [maximal value of $\alpha_{xy}(T)$] and $\alpha(300\ \mathrm{K})$ for deformed and doped Fe_3Ga.

Crystal structure	$\alpha_{\max}$ ($\mathrm{A\,K^{-1}\,m^{-1}}$)	$\alpha(300\ \mathrm{K})$ ($\mathrm{A\,K^{-1}\,m^{-1}}$)
Cubic Fe_3Ga	1.7	1.7
$Fe_3Ga_{0.95}Ge_{0.05}$	2.5	2.5
$Fe_3Ga_{0.9}Ge_{0.1}$	3.0	3.0
$Fe_3Ga_{0.8}Ge_{0.2}$	3.3	3.0
$Fe_3Ga_{0.95}Zn_{0.05}$	0.8	0.6
$Fe_3Ga_{0.9}Zn_{0.1}$	−0.7	−0.6
$Fe_3Ga_{0.8}Zn_{0.2}$	−2.6	−2.6
tetra, $c > c_0$, 0.5%	2.1	2.1
tetra, $c > c_0$, 1.0%	2.1	2.0
tetra, $c > c_0$, 1.5%	2.4	2.2
tetra, $c < c_0$, 0.5%	0.9	0.8
tetra, $c < c_0$, 1.0%	−0.6	−0.1
tetra, $c < c_0$, 1.5%	−0.9	−0.9

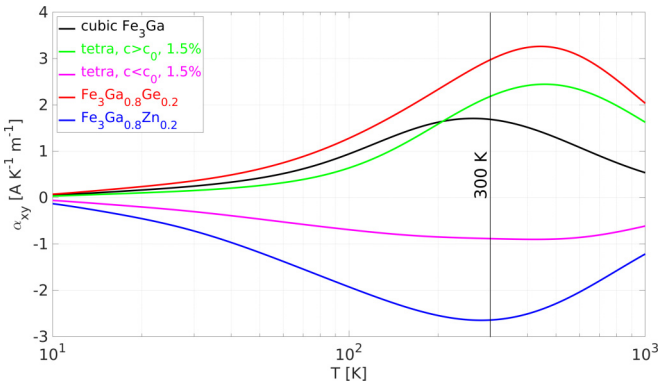

FIG. 3. Temperature dependence of the anomalous transverse thermoelectric coefficient α.

B. Deformation

Two general cases of deformation were considered, namely compressive and tensile strain. With compressive strain, the in-plane lattice parameter is shortened by 0.5%, 1.0%, and 1.5%, while preserving the total volume of the unit cell. As the out-of-plane lattice parameter gets larger, this case is denoted by tetra, $c > c_0$.

In the tensile strain case, the in-plane lattice parameter is extended by 0.5%, 1.0%, and 1.5%, denoted by tetra, $c < c_0$. In both cases, the crystal structure changes from cubic (space group *Fm*-3*m*, No. 225) to tetragonal (*I*4/*mmm*, No. 139). The respective band structures are shown in Fig. S1 in the Supplemental Material [29].

The results are shown in Fig. 4 and summarized in Table I. In both cases, deformation leads to smoothening of the spectrum. However, while the tensile strain tends to cancel out the effect, compression leads to a significant increase of ANE. Therefore, in thin film applications substrates with smaller lattice parameters should be considered.

The change of the AHC spectra under deformation is definitely not trivial, since with lowered symmetry the entire band structure is different. In order to provide some basic insight into this matter, we shall study the sources of the anomalous behavior in the Brillouin zone of cubic Fe_3Ga followed by the analysis of the effect of doping and applied strain.

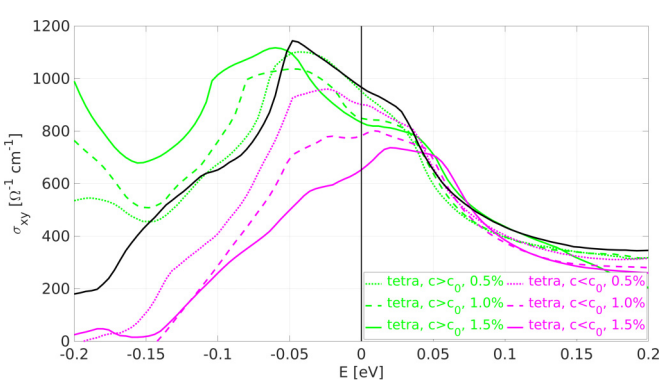

FIG. 4. AHC spectrum for deformed Fe_3Ga crystal structure. Black line represents spectrum of undeformed bulk AHC.

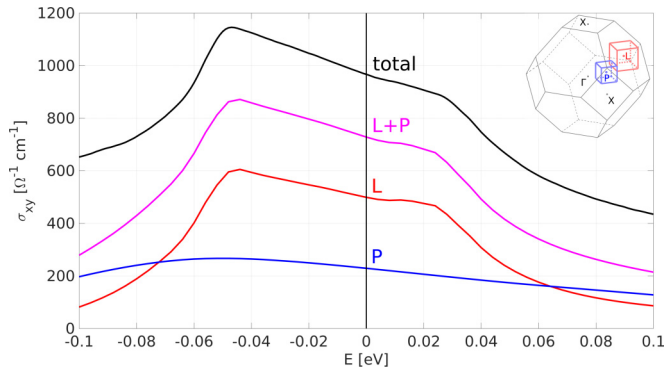

FIG. 5. Spectrum of the anomalous Hall conductivity in Fe_3Ga as a function of the Fermi energy position. The total value is represented by black line. Red, blue, and magenta lines correspond to contributions to conductivity from L, P, and L+P cubes, respectively. In the inset, the Brillouin zone is depicted with L and P cubes.

III. ANALYSIS OF THE ANE SPECTRA

In this section we analyze the ANE spectrum to identify the origin of the effect. On the standard k path through the reciprocal space [see Fig. 1(a)], there is only single major source of the Berry curvature in the vicinity of point L as identified by other authors [18]. However, the inspection of the Brillouin zone reveals that there are two distinct contributions that cover the majority of AHC. Apart from the aforementioned L point, a strong source of the Berry curvature appears in the general position around point P = [0.55, 0.15, 0.25], expressed in the relative Cartesian coordinates.

Both sources can be numerically separated and their partial spectra (integrated inside the respective cubes, including multiplicity) are shown in Fig. 5 along with the total anomalous conductivity obtained by integration of the Berry curvature over the entire Brillouin zone via Eq. (2) in the energy range −0.1 to 0.1 eV. By modifying the value of the Fermi energy, only the positions of the Fermi surfaces change which is reflected by $f_n(\mathbf{k})$ entering the integral through $\mathbf{\Omega}^{\mathrm{occ}} = \Sigma_n f_n(\mathbf{k})\mathbf{\Omega}^n(\mathbf{k})$. The Berry curvature vector field of individual bands $\mathbf{\Omega}^n(\mathbf{k})$ is not affected by the modification of electron occupancy.

Together, both partial spectra cover over 70% of the total anomalous conductivity throughout the entire energy range and are separated from the total by a mere constant.

In the following, we shall analyze both contributions separately, identify the contributing Berry curvature flows, and inspect the evolution of the Fermi surface with the Fermi level position.

A. Contribution originating in cube P

First, the contribution from the cube centered at point P is analyzed [see Fig. 6(c)]. The energy dependence of the anomalous conductivity in this region is shown in Fig. 6(a). It repeats 16 times in the Brillouin zone due to symmetry and describes 21% of the total anomalous conductivity. Upon close inspection, it is found that this region features only two bands, namely bands 18 and 19. The Berry curvature of band 18 is depicted in Fig. 6(d), while the Berry curvature of band 19 flows in the opposite direction providing $\mathbf{\Omega}^{18} + \mathbf{\Omega}^{19} = 0$ in

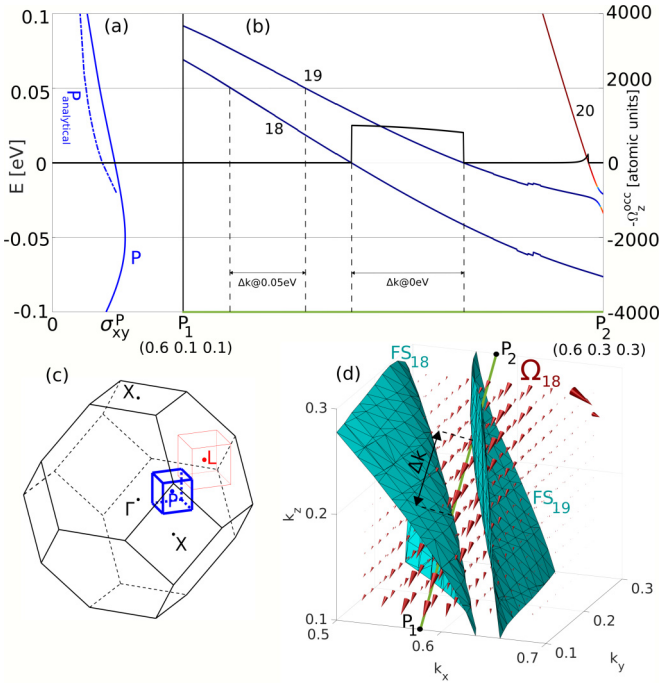

FIG. 6. (a) AHC spectrum originated in cube P. The dash-dotted blue line corresponds to the analytical approximation of the P contribution [Eq. (4)]. (b) Band structure in the direction of the Berry curvature flow with the z component of the Berry curvature over occupied states $\Omega_z^{\mathrm{occ}} = \Sigma_n f_n \Omega_z^n$ that is approximately equal to Ω_z^{18} in the region between both Fermi surfaces. The reciprocal distance Δk at two Fermi level positions is indicated. (c) Brillouin zone with the position of cube P. (d) Flow of the Berry curvature of band 18 in cube P. The flux of the flow equals $2\pi/3$. Fermi surfaces for bands 18 and 19 at $E = 0$ eV are depicted, Berry curvature between the surfaces contributes to AHC. The green line represents the path along which the band structure in (b) is depicted.

this part of the BZ. It is of particular interest to plot the band structure in the direction of the flow (along the green P_1P_2 line) which is shown in Fig. 6(b).

Both bands are split by the crystal field even without SOI and do not form nodal lines. SOI only further increases the energy split. Since $\mathbf{\Omega}^{18} + \mathbf{\Omega}^{19} = 0$ and $\mathbf{\Omega}^{\mathrm{occ}} = \Sigma_n f_n \mathbf{\Omega}^n$, it is clear that only the Berry curvature in the region between the Fermi surfaces of bands 18 and 19 contributes to the anomalous conductivity. Furthermore, the flow is localized along the green P_1P_2 line; hence the value of the conductivity can be approximated by an analytical formula [30]:

$$\sigma_{xy}^{\mathrm{P}} = -\frac{e^2}{\hbar}\frac{1}{(2\pi)^3}\Phi^{18}\Delta k\cos\varphi, \quad \cos\varphi = \hat{\Omega}\cdot\hat{z}. \tag{4}$$

The Berry curvature flux is $\Phi^{18} = \int d\mathbf{S}\cdot\mathbf{\Omega}^{18} = 2\pi/3$ highlighting the threefold rotational symmetry present in the crystal. Δk is the reciprocal distance between the respective Fermi surfaces in the direction of the Berry curvature flow. In the depicted case $\Delta k = 0.0417$ bohr^{-1} and $\cos\varphi = -1/\sqrt{2}$, as the Berry curvature flows in the $[0\bar{1}\bar{1}]$ direction. This provides a contribution from a single 1D flow $\sigma_{xy}^{\mathrm{P}} = 11.5$ $(\Omega\,\mathrm{cm})^{-1}$. Due to symmetry, this contribution appears sixteen times in the BZ with the total strength of 184 $(\Omega\,\mathrm{cm})^{-1}$,

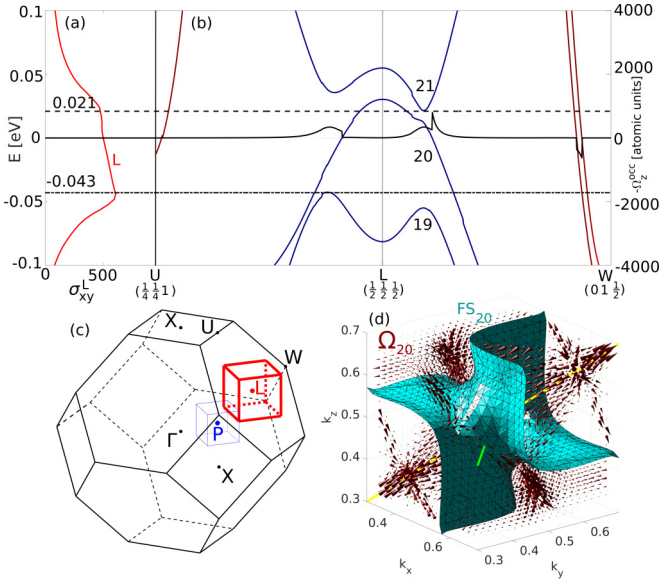

FIG. 7. (a) AHC spectrum originated in cube L. (b) Band structure along the ULW path. The dashed and dash-dotted lines at −0.043 eV and 0.021 eV, respectively, correspond to both turning points in the spectrum. (c) Brillouin zone with the position of cube L. (d) Flow of the Berry curvature and Fermi surface of band 20 in cube L. Berry curvature outside the surface contributes to AHC. Green and yellow lines highlight the W-L and Γ-L directions, respectively. Their intersection is the L point.

representing about 80% of the numerically obtained value in cube P, as the Fermi surfaces are not exactly parallel when crossing the Berry curvature flow.

It is apparent from the band structure in Fig. 6(b) that the distance Δk changes with varying position of the Fermi level which is one of the ways to obtain the nonzero derivative and hence nonzero ANE. The results of the analytical formula for σ_{xy}^{P} are represented by the dash-dotted blue line in Fig. 6(a). They are not provided in the entire range as for energies below −0.02 eV a third band (20) emerges and acts as an additional source of Berry curvature.

B. Contribution originating in cube L

The second dominant source of the Berry curvature is located in the vicinity of the L point [Fig. 7(c)]. The energy dependence of the anomalous conductivity in this region is shown in Fig. 7(a). It repeats 4 times in the Brillouin zone due to symmetry and describes 52% of the total anomalous conductivity. Even though there are no degeneracies present, the close proximity of the band triplet leads to strong hybridization and generates large Berry curvatures.

The sum of the Berry curvatures of the band triplet $\mathbf{\Omega}^{19} + \mathbf{\Omega}^{20} + \mathbf{\Omega}^{21}$ equals zero in cube L. Therefore, if all three bands are either occupied or unoccupied, they do not contribute to the anomalous effects. The dashed and dash-dotted lines in the band structure Fig. 7(b) mark the energies where the upper and lower band gets occupied and unoccupied, respectively, and correspond to both turning points in the spectrum Fig. 7(a).

The anomalous effects inside energy region −0.043 eV to 0.021 eV (between the dashed and dash-dotted lines) are

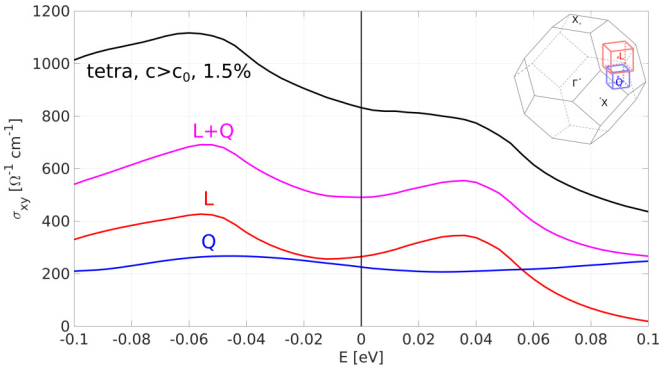

FIG. 8. AHC spectrum of compressed Fe_3Ga with partial contributions.

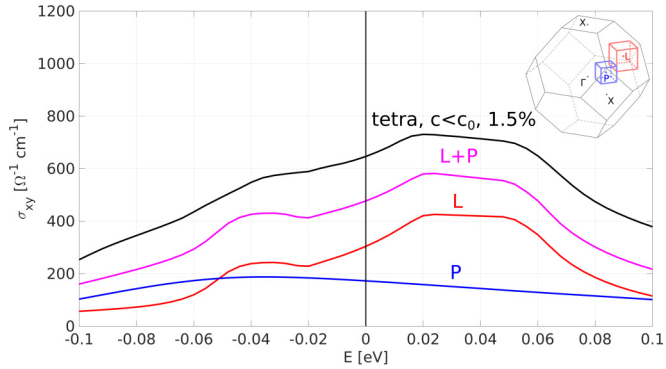

FIG. 9. AHC spectrum of stretched Fe_3Ga with partial contributions.

governed solely by varying occupation of the middle band 20. The Berry curvature structure of this band is complicated and can be seen in Fig. 7(d). The Berry curvature in the occupied region contributes to the anomalous conductivity. With increasing Fermi energy, the Fermi surface shrinks inward enabling other parts of the Berry curvature flows to contribute. There are flows in many directions; some add to and some subtract from the total value. Thus, precise geometry and width of the individual flows matter and the value of AHC steadily decreases with increasing energy leading to a nonzero contribution to ANE.

C. Partial contributions under deformation

Under compressive (Fig. 8) and tensile (Fig. 9) strain, the partial contribution analysis shows that the vicinity of point L dominates both AHC spectra and determines solely their overall shape around the Fermi level. Unfortunately, a detailed investigation of Berry flows did not provide any additional insight; therefore we present numerical results only. For more information, see the Supplemental Material [29], where band structures for all discussed cases (Fig. S1) and also the Berry curvature flows around point L (Fig. S2) are shown.

In the compressed case, the P contribution vanishes (as the energy distance between respective bands increases; see Fig. S3 in the Supplemental Material [29]). However, a new contribution arises around point Q = [0.5, 0.5, 0.15] with similar strength (see inset of Fig. 8). Only in the compressed case, the Fermi level falls exactly between two hybridizing bands (see Fig. S4 in the Supplemental Material [29]).

The overall character of the spectra is preserved under deformation, with both fundamental peaks approximately at the same energy position, suggesting a small change in the electronic structure. On the other hand, the strength of individual peaks decreases, suggesting a change of spin-orbit splitting between respective bands leading to modifications of the Berry curvature vector field.

IV. CONCLUSION

We performed *ab initio* calculations of several Fe_3Ga structures modified by deformation and doping. We showed that compressive strain leads to a significant increase of α_{xy} and hence should be sought for in applications. Doping modeled via the virtual crystal approximation effectively moves the position of the Fermi level and enables additional tuning of the α_{xy} value. For example, the model predicts that 20% of Ge doping almost doubles the ANE.

Furthermore, we analyzed the origin of the ANE in DO_3-ordered Fe_3Ga and identified two dominant sources in the Brillouin zone related to the Berry curvature flow in the vicinity of the Fermi level. Note, however, that the analysis presented in this work covers only the intrinsic part of the anomalous Nernst effect and omits scattering mechanisms.

ACKNOWLEDGMENTS

This work was supported by the Czech Science Foundation (GACR), Grant No. 22-21974S, and by the Ministry of Education of the Czech Republic by the OP RDE programme, Project No. Matfun CZ.02.1.01/0.0/0.0/15_003/0000487.

[1] Y. Yao, L. Kleinman, A. H. MacDonald, J. Sinova, T. Jungwirth, D.-S. Wang, E. Wang, and Q. Niu, Phys. Rev. Lett. **92**, 037204 (2004).
[2] N. Nagaosa, J. Sinova, S. Onoda, A. H. MacDonald, and N. P. Ong, Rev. Mod. Phys. **82**, 1539 (2010).
[3] D. Xiao, M.-C. Chang, and Q. Niu, Rev. Mod. Phys. **82**, 1959 (2010).
[4] B. Ernst, R. Sahoo, Y. Sun, J. Nayak, L. Müchler, A. K. Nayak, N. Kumar, J. Gayles, A. Markou, G. H. Fecher, and C. Felser, Phys. Rev. B **100**, 054445 (2019).
[5] C. Helman, A. Camjayi, E. Islam, M. Akabori, L. Thevenard, C. Gourdon, and M. Tortarolo, Phys. Rev. B **103**, 134408 (2021).
[6] D. Xiao, Y. Yao, Z. Fang, and Q. Niu, Phys. Rev. Lett. **97**, 026603 (2006).
[7] A. Sakai, Y. P. Mizuta, A. A. Nugroho, R. Sihombing, T. Koretsune, M.-T. Suzuki, N. Takemori, R. Ishii, D. Nishio-Hamane, R. Arita, P. Goswami, and S. Nakatsuji, Nat. Phys. **14**, 1119 (2018).
[8] John Kerr, Mag. J. Sci. **3**, 321 (1877).

[9] R. Silber, O. Stejskal, L. Beran, P. Cejpek, R. Antoš, T. Matalla-Wagner, J. Thien, O. Kuschel, J. Wollschläger, M. Veis, T. Kuschel, and J. Hamrle, Phys. Rev. B **100**, 064403 (2019).
[10] G. J. Snyder and E. S. Toberer, Nat. Mater. **7**, 105 (2008).
[11] G. Hu, H. Edwards, and M. Lee, Nat. Electron. **2**, 300 (2019).
[12] M. Ikhlas, T. Tomita, T. Koretsune, M.-T. Suzuki, D. Nishio-Hamane, R. Arita, Y. Otani, and S. Nakatsuji, Nat. Phys. **13**, 1085 (2017).
[13] E. Liu, Y. Sun, N. Kumar, L. Muechler, A. Sun, L. Jiao, S.-Y. Yang, D. Liu, A. Liang, Q. Xu, J. Kroder, V. Süß, H. Borrmann, C. Shekhar, Z. Wang, C. Xi, W. Wang, W. Schnelle, S. Wirth, Y. Chen, S. T. B. Goennenwein, and C. Felser, Nat. Phys. **14**, 1125 (2018).
[14] J. Noky, Q. Xu, C. Felser, and Y. Sun, Phys. Rev. B **99**, 165117 (2019).
[15] S. N. Guin, P. Vir, Y. Zhang, N. Kumar, S. J. Watzman, C. Fu, E. Liu, K. Manna, W. Schnelle, J. Gooth, C. Shekhar, Y. Sun, and C. Felser, Adv. Mater. **31**, 1806622 (2019).
[16] S. Minami, F. Ishii, M. Hirayama, T. Nomoto, T. Koretsune, and R. Arita, Phys. Rev. B **102**, 205128 (2020).
[17] J. Noky, Y. Zhang, J. Gooth, C. Felser, and Y. Sun, npj Comput. Mater. **6**, 77 (2020).
[18] A. Sakai, S. Minami, T. Koretsune, T. Chen, T. Higo, Y. Wang, T. Nomoto, M. Hirayama, S. Miwa, D. Nishio-Hamane, F. Ishii, R. Arita, and S. Nakatsuji, Nature (London) **581**, 53 (2020).
[19] T. Chen, S. Minami, A. Sakai, Y. Wang, Z. Feng, T. Nomoto, M. Hirayama, R. Ishii, T. Koretsune, R. Arita, and S. Nakatsuji, Sci. Adv. **8**, eabk1480 (2022).
[20] S. Nakatsuji and R. Arita, Annu. Rev. Condens. Matter Phys. **13**, 119 (2022).
[21] H. Reichlova, R. Schlitz, S. Beckert, P. Swekis, A. Markou, Y.-C. Chen, D. Kriegner, S. Fabretti, G. Hyeon Park, A. Niemann, S. Sudheendra, A. Thomas, K. Nielsch, C. Felser, and S. T. B. Goennenwein, Appl. Phys. Lett. **113**, 212405 (2018).
[22] Y. Hamada, Y. Kurokawa, T. Yamauchi, H. Hanamoto, and H. Yuasa, Appl. Phys. Lett. **119**, 152404 (2021).
[23] H. Nakayama, K. Masuda, J. Wang, A. Miura, K.-i. Uchida, M. Murata, and Y. Sakuraba, Phys. Rev. Mater. **3**, 114412 (2019).
[24] C. Paduani and C. Bormio-Nunes, J. Appl. Phys. **109**, 033705 (2011).
[25] P. Blaha, K. Schwarz, G. K. H. Madsen, D. Kvasnicka, and J. Luitz, *WIEN2K, An Augmented Plane Wave + Local Orbitals Program for Calculating Crystal Properties* (Karlheinz Schwarz, Technische Universität Wien, Austria, 2001).
[26] C. Ambrosch-Draxl and J. O. Sofo, Comput. Phys. Commun. **175**, 1 (2006).
[27] J. P. Perdew, K. Burke, and M. Ernzerhof, Phys. Rev. Lett. **77**, 3865 (1996).
[28] M. Matyunina, M. Zagrebin, V. Sokolovskiy, and V. Buchelnikov, EPJ Web Conf. **185**, 04013 (2018).
[29] See Supplemental Material at http://link.aps.org/supplemental/10.1103/PhysRevMaterials.7.084403 for more details on the electronic structure of deformed Fe_3Ga and the Berry curvature analysis of individual contributions to the anomalous effects.
[30] O. Stejskal, M. Veis, and J. Hamrle, Sci. Rep. **12**, 97 (2022).